


Topological and conventional phases of a three-dimensional electronic glassPrateek Mukati,^{*} Adhip Agarwala,[†] and Subhro Bhattacharjee[‡]*International Centre for Theoretical Sciences, Tata Institute of Fundamental Research, Bengaluru 560089, India* (Received 15 September 2019; revised manuscript received 21 December 2019; published 27 January 2020)

We investigate a symmetry-protected Z_2 topological electron glass, a glassy equivalent of the Z_2 topological band insulator in crystalline systems, and uncover associated quantum phase transitions in this three-dimensional amorphous network of atoms. Through explicit numerical calculations of the Witten effect, we show that the Z_2 glass is characterized by an anomalous electromagnetic response, i.e., it can host dyons with $\frac{1}{2}$ electronic charge. We further study, using a variety of numerical diagnostics including such electromagnetic responses, the phase transitions of the Z_2 glass into a metallic and/or a trivial insulating phase. We find that the phase transitions here are governed by subtle features of mobility edges and “spectral inversion” which are possibly unique to structurally amorphous systems. Our results provide a concrete setting to understand the general underpinnings of such phases, where strong structural disorder interplays with symmetry-protected topological order.

DOI: [10.1103/PhysRevB.101.035142](https://doi.org/10.1103/PhysRevB.101.035142)**I. INTRODUCTION**

Symmetry-protected topological (SPT) phases [1–8] of electrons, even in the weak coupling limit, in amorphous and structurally glassy systems provide for the interplay of structural disorder, residual global symmetries, and patterns of quantum entanglement on the many-body electronic states [9,10]. A particularly interesting and recent setting to explore such physics occurs in the three-dimensional Z_2 free-fermion SPTs [e.g., the topological band insulators (TBI)], protected by time-reversal symmetry (TRS) and particle-number conservation, in simple hopping models of spin 1/2 electrons on a structurally amorphous network [9].

Starting with an underlying crystal, the role of potential disorder in three-dimensional Z_2 TBI and associated disorder-driven quantum phase transitions have been investigated using a variety of methods [11–19]. Interestingly, in this context Ref. [20] pointed out that even a clean metallic system can be driven by potential disorder to show topological physics, albeit in a narrow parameter regime. However, possibilities of realizing such topological phases [9] in three-dimensional *electron glass*, i.e., in a completely random network, provide a distinct new setting to access the underlying issues related to the characterization of such SPTs which are intrinsically beyond band theory [21–43]. This, in turn, allows one to explore questions related to novel quantum phase transitions driven by structural disorder [44–48] in these amorphous systems. Indeed, recent extensive numerical calculations [49] show various features, mostly related to the nature of quantum phase transitions, in a number of two-dimensional topological phases in structurally disordered systems that are distinct from conventional crystalline systems with potential disorder.

This calls for a comprehensive characterization of electronic topological phases and phase transitions in three-dimensional amorphous networks, which is presently missing. In particular, we pose the question, given a random set of atomic sites, with no semblance of a lattice: What generic (topological) phases can exist in three dimensions and what can be said about the nature of associated phase transitions out of such a phase? Indeed, the possibility of realizing such electronic phases in structurally glassy systems opens up a plethora of new questions related to their stability to interactions and slow relaxation dynamics of the underlying network.

In this paper, we take important steps to address both these questions in context of a three-dimensional Z_2 topological glass (TG) using a combination of extensive numerical diagonalization of the Hamiltonian (see below) and ideas from localization physics. We perform extensive characterization of a three-dimensional amorphous Z_2 free-fermionic SPT through its characteristic quantized electromagnetic response, the so-called Witten effect [50–52], which serves as an effective diagnostic of the nontrivial electronic state. While such an effect is present in crystalline three-dimensional TBIs where it has been analyzed [52] and corroborates with band topology based calculation of Z_2 invariants; in absence of the latter for, e.g., in case of TG, the detection of Witten effect and its stability as well as its annihilation becomes central to characterizing the phase. We further study the complete phase diagram to understand the possible phase transitions out of this SPT phase. Our central result is shown in Fig. 1 where our numerical calculations show that by varying the microscopic parameters (discussed below) we can access two generic classes of transitions out of the TG: (1) to a metallic phase which subsequently becomes an Anderson insulator with or without a spectral gap, and (2) direct transition to an Anderson insulator with a spectral gap which we refer to as a trivial spectral insulator (SI) in the rest of this paper. Interestingly, the SI of this work is the same state as the extensively studied structural glass with electronic spectral gaps [53–58]. We provide a

^{*}prateek.mukati@icts.res.in[†]adhip.agarwala@icts.res.in[‡]subhro@icts.res.in

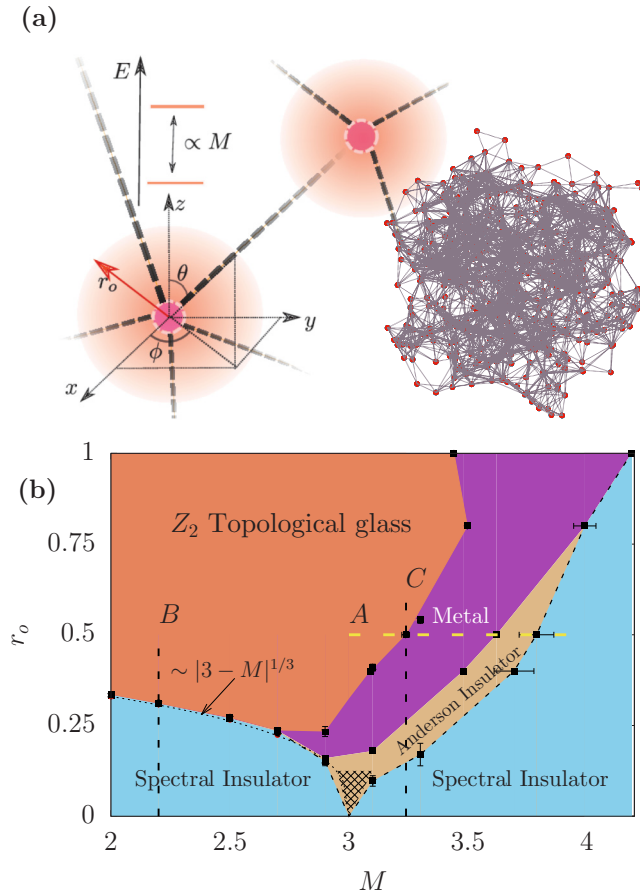


FIG. 1. Model and Phase Diagram: (a) A model of amorphous glass is shown with a random distribution of sites in three dimensions as introduced in [9]. While r_0 characterizes the “Bohr’s radius” of the atoms, M is proportional to the atomic spectral gap between the two atomic orbitals per site (see text). (b) Phase diagram for a half-filled system in the $r_0 - M$ parameter space. A–C are parameter cuts discussed later in the text.

descriptive understanding of such transitions via the behavior of mobility edges and relating to ideas of “spectral” inversion.

II. MODEL FOR AMORPHOUS Z_2 INSULATOR IN THREE SPATIAL DIMENSIONS

Our starting point is the the hopping Hamiltonian introduced in Ref. [9]:

$$H = \sum_{I\alpha\sigma} \sum_{J\beta\sigma'} t_{\alpha\beta}^{\sigma\sigma'}(\mathbf{r}_{IJ}) C_{I,\alpha,\sigma}^\dagger C_{J,\beta,\sigma'}, \quad (1)$$

where $C_{I,\alpha,\sigma}$ is the annihilation operator for a pair (orbitals $\alpha, \beta = s, p$) of spin- $\frac{1}{2}$ ($\sigma, \sigma' = \uparrow, \downarrow$) fermionic Kramers doublets at every site (labeled by I, J) of a random network of “atoms” embedded in three spatial dimensions, as is schematically shown in Fig. 1(a). \mathbf{r}_{IJ} is the vector from site I to site J . Centrally, for $I \neq J$, the hopping amplitude has the form $t_{\alpha\beta}^{\sigma\sigma'}(\mathbf{r}) = t(r)T_{\alpha\beta}^{\sigma\sigma'}(\hat{\mathbf{r}})$ where $T_{\alpha\beta}^{\sigma\sigma'}(\hat{\mathbf{r}})$ captures the angular dependence of hopping (see Appendix A) and $t(r) = \Theta(R - r)e^{-(r-r_0)/r_0}$ determines the distance dependence. Further, given number of sites N , embedded in a spatial volume

$V = L^3$ (L is the linear dimension), the essential length scale of average distance between sites $a_0 = (\frac{V}{N})^{1/3}$ is set to 1 in the rest of the paper. Finally, we consider the system at half-filling, i.e., the number of total electrons are $2N$.

In the above units, $t(r)$ encodes two comparative length scales r_0 and R . The former, a “Bohr’s radius,” quantifies the essential size of the atomic orbitals while the latter enforces a hard cutoff that keeps the hopping short ranged even when r_0 is tuned. Note that it is important to keep $R \ll L$ in order to treat the system as three-dimensional all the way up to $r_0 \sim R$. Indeed, for $r_0 \sim R \sim L$ the system reduces to a zero-dimensional “quantum dot” with many *internal* states. The structure of $t_{\alpha\beta}^{\sigma\sigma'}(0) \equiv \epsilon_{\alpha\beta}$ dictates the onsite energy of the system which is tuned by a single “mass” parameter M (see Appendix A). Thus, for a given R , both r_0 and M determine the phase of the system which can then be varied to yield the phase diagram (Fig. 1). Broadly, M controls the spectral gap while r_0 governs the strength of hopping between randomly placed atoms within a sphere of radius R , hence simultaneously controlling the physics of delocalization as well as effective disorder. Indeed, Ref. [9] showed the existence of delocalized surface states for a particular set of parameters in this system, suggesting a Z_2 topological glass phase.

III. WITTEN EFFECT

A comprehensive characterization of the Z_2 insulator in three dimensions can be obtained by the Witten effect. This can be understood from the effective low-energy Lagrangian of a time-reversal symmetric insulator which contains an axion contribution of $\Delta\mathcal{L} = \frac{\alpha}{4\pi^2}\theta\mathbf{E}\cdot\mathbf{B}$ (α being the fine-structure constant) in addition to the usual Maxwell action. Here, the axion angle θ is $0[\text{mod}(2\pi)]$ (trivial SI) or $\pi[\text{mod}(2\pi)]$ (TG) due to TRS. Due to the nonzero axion angle, when a magnetic monopole (m) is placed inside a Z_2 insulator, it binds a half-odd integer electric charge (e) with it to form a *dyon* [50,51,59]. Indeed, properties of such *dyons* can lead to identification of new SPT phases in presence of interactions [60–66].

To investigate this effect in a topological glass, we introduce a unit magnetic monopole (see Appendix B) which couples to the electrons through minimal coupling $t_{\alpha\beta}^{\sigma\sigma'}(\mathbf{r}_{IJ}) \rightarrow e^{iA_{IJ}} t_{\alpha\beta}^{\sigma\sigma'}(\mathbf{r}_{IJ})$ where A_{IJ} is the total Peierls phase between sites I and J . This leads to a shift in the electronic charge density at every site [see Figs. 2(a) and 2(b)]. The cumulative electronic charge difference (compared to the case without the monopole) inside a sphere of radius r measured from the location of the monopole $\equiv Q_D(r)$ is also shown in Fig. 2(c) for a half-filled system. Noticeably, $Q_D(r)$ saturates to a value of $\frac{1}{2}$ within numerical accuracy, illustrating realization of Witten effect in an amorphous glass. That this half of the charge had distributed from the boundary is evident by the fall of Q_D to zero as r approaches L , showing that the compensating half of the charge lives in the boundary. Fitting the region of $r < L$ to a functional form of $\sim e_D(1 - e^{-(r-a)/\xi})$ estimates the dyon charge e_D and corresponding “size” of the dyon $\equiv l_D = \xi + a$ [see Fig. 2(c)]. However, the value of dyon length and the way e_D transits from 0 to 0.5 (modulo 1) is configuration sensitive [see Appendix B and Fig. 5(a)].

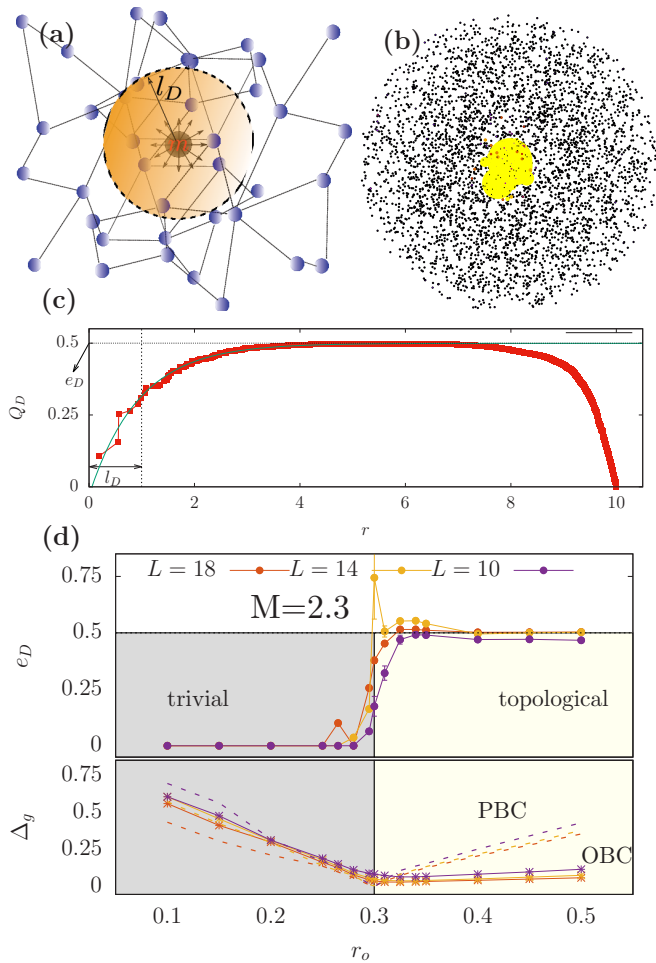


FIG. 2. Witten effect: (a), (b) Inclusion of a magnetic monopole leads to a redistribution of the charge throughout the amorphous network. (c) For $M = 0.0$ and $r_0 = 1.0$ the value of the accumulated charge is plotted as a function of distance r showing that the charge saturates to a value of $e_D \sim \frac{1}{2}$. (d) Variation of the dyon charge e_D as a function of r_0 showing a transition from a trivial spectral insulator to a topological glass phase. The corresponding spectral gap (Δ_g) for both the amorphous sphere (star with solid lines) and for an amorphous cubic system with periodic boundary condition (dotted lines) is shown signaling a bulk gap closing.

IV. PHASE DIAGRAM

The Witten effect not only characterizes the TG, but as shown in Fig. 2(d), the quantized electric charge $Q_D = 1/2$ of the dyon disappears across transition to a trivial spectral insulator. Not surprisingly, the disappearance of the Witten effect coincides with the closing of the bulk spectral gap for a system with periodic boundary conditions as is evident from Fig. 2(d). Such a bulk gap closing is essential for the axion angle to change and thereby signaling the phase transition. This immediately raises the general question of the characterization of nature of the phases and associated transitions out of the TG in the whole (r_0, M) plane. We perform exact diagonalizations over ~ 200 configuration realizations for system sizes $L = 8-14$ to calculate, in addition to the Witten effect, the spectral gap, the inverse participation ratio (IPR), and the orbital nature of the states close to the Fermi

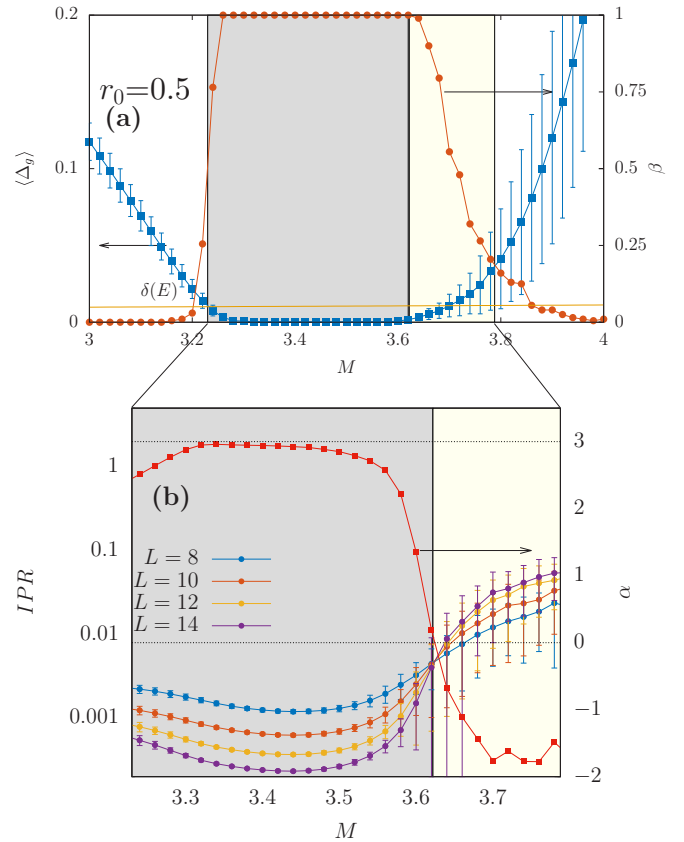


FIG. 3. Intermediate phases: (a) Configuration-averaged spectral gap Δ_g as a function of M for $L = 14$ and number of configurations $N_c = 200$ (cut A in Fig. 1). Also shown is the behavior of β , defined as the fraction of configurations which have an energy state within a small window $\delta(E)$ near the Fermi energy (see text). (b) Configuration-averaged IPR is shown for different system sizes. Fitting these values to a form of $1/L^\alpha$, behavior of α is shown as a function of M . In the metallic regime $\alpha \sim 3$. The rare-region-dominated Anderson localization shows anomalous scaling with $\alpha < 0$ ($N_c = 200$).

level to obtain the phase diagram plotted in Fig. 1(b). To implement periodic boundary condition in any direction, we allow fermionic hopping in a “repeated” configuration with distances modulo L in all directions and identify equivalent sites.

To this end, let us concentrate on a typical cut shown as line A in Fig. 1 at a constant $r_0 = 0.5$ as a function of M and consider states within a small window of states [$\delta(E) = 10 \times E_{bw}/(4N)$ also shown in Fig. 3(a)] around the Fermi level, where E_{bw} is the bandwidth of the spectrum. In Fig. 3(a), we plot the configuration-averaged spectral gap as a function of M . The finite spectral gap region for $M \lesssim 3.2$ is the Z_2 topological glass phase with axion angle $\theta = \pi$ leading to half-quantized Witten effect discussed above while for the regime $3.2 \lesssim M \lesssim 3.8$ where the spectral gap is zero (within standard deviation) represents a gapless phase. Beyond $M \gtrsim 3.8$, the spectral gap reopens and this is a trivial spectral insulator with axion angle $\theta = 0$ (not shown).

At this point, it is important to note that for a finite $N_c = 100-400$ number of independent configurations, we can

calculate the subset of configurations N_I that lead to at least one state within the above energy window of $\delta(E)$. The fraction of such states $\beta = N_I/N_c$ is also plotted in Fig. 3(a) and we find that while for the transition from the Z_2 topological glass to gapless phase, the fraction quickly goes to one from zero, the change is much more gradual for the transition from gapless phase to the trivial spectral insulator on the other side. In parallel, our data suggest stark asymmetry of the magnitude of the standard deviation on the value of the spectral gap on either side of the gapless window. While the magnitude of the standard deviation is much smaller on the Z_2 topological glass side or on the gapless region, it is much bigger on the other end, suggesting that the spectral gap has a wider distribution near the transition between the gapless state and the trivial spectral insulator (see Appendix C). This observation is further reinforced by the analysis of the configuration-averaged IPR in the gapless regime ($3.2 \lesssim M \lesssim 3.8$) as shown in Fig. 3(b). We find that configuration-averaged typical states in the parameter range $3.2 \lesssim M \lesssim 3.6$ have an IPR that scales with system as $\sim 1/L^\alpha$ where $\alpha \sim 3$ (see Fig. 3), characteristic of a *metallic* phase. However, in the narrow window $3.6 \lesssim M \lesssim 3.8$, the IPR behavior is consistent with a negative α when fitted to the above form with $M = 3.6$ being the point where $\alpha = 0$ and changes sign and becomes negative! Indeed, it is interesting to note the prominent crossing of IPRs of the different system sizes at $M = 3.6$. Again, there are large values of standard deviation in the regime $M \gtrsim 3.6$ where α is close to zero. This is typical of formation of localized states near a metal Anderson insulator transition suggesting the onset of Anderson localization [44,47].

In the light of possible localization physics at play, the negative α finds a natural explanation. That with increasing system size, probability of finding *more* dominantly localized states increases, is a feature attributed to rare regions that are known to occur in the Lifshitz tails of a disordered band. Given the two-band character of our energy spectrum, the states near the Fermi energy are indeed these rare regions belonging to both the upper and lower band, thereby providing for the surprising feature in the IPR as mentioned above. With further increase in M , even the Lifshitz tails move beyond the band spectrum, leading to a trivial spectral insulator as seen in Fig. 3.

In order to further understand the general phases and their transitions, we now investigate the orbital behavior and the energy spectrum of a single amorphous configuration as a function of r_o for two cuts (B and C) as shown in Fig. 1(b). Both these vertical cuts have a simple trivial atomic insulator limit when $r_o = 0$ where the network degenerates to disconnected atoms with the onsite *atomic orbitals* leading to two isolated spin-degenerate states on each atom separated by an onsite energy $|3 - M|$ in the present parametrization. At half-filling, this gives a trivial atomic insulator (unless $M = 3$ where it is a highly degenerate state susceptible to perturbations leading to the breakdown of our numerical accuracy as mentioned in Fig. 1). For a fixed finite R , tuning $r_o > 0$ (at a constant M) modulates the strength of the connectivity of the electronic orbitals on different atoms of the disordered network (see Appendix D). While the trivial atomic insulator is stable to small $r_o > 0$, the energy eigenstates are no longer strictly onsite, leading to the formation of two bands of

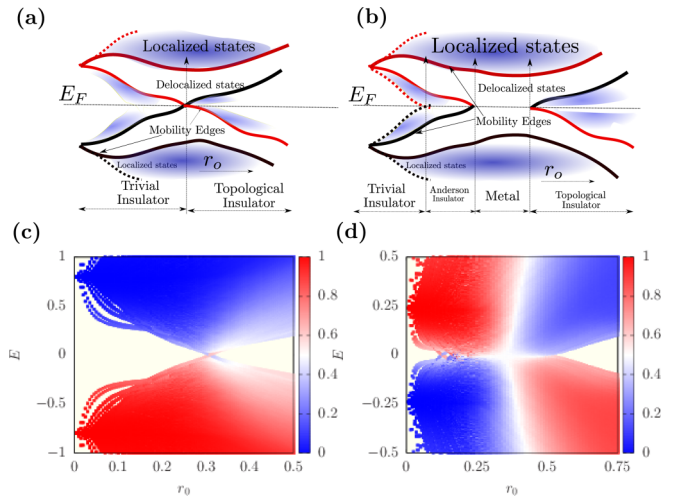


FIG. 4. Phase transitions: (a) Schematic showing that the transition across the cut B ($M = 2.2$) and (b) across cut C ($M = 3.24$) of the phase diagram as shown in Fig. 1. The schematic shows the various intermediate phases which are encountered. (c), (d) The behavior of the energy spectrum as a function of r_o for a particular periodic configuration ($R = 2$, $L = 14$). The color bar shows the s orbital character of each of the state. While in cut B it is the highest occupied orbital which contributes to shifting of the spectral weight, in cut C many low-energy states contribute to this feature due to an intervening metallic phase.

fully localized states around energies $\pm|3 - M|$. On further increasing r_o , the states in the middle of each of these bands become delocalized, giving rise to two pairs of mobility edges which approach the Fermi level with increasing r_o and eventually leading to the closing of the spectral gap at a critical $r_o = r_{0B(C)}$ for the cut B(C). This is shown in Fig. 4(b). The extent of the delocalization of the states near the Fermi level is characterized by their IPR, which is shown in Appendix C.

For cut B, the spectral gap immediately (within our numerical resolution) reopens on cross r_{0B} . However, the orbital nature of the occupied orbitals close to Fermi energy changes across the bulk gap closing transition, but the bulk does not change significantly. In this sense, we have an inverted spectral gap for $r_o > r_{0B}$ (compared to the atomic insulator) which is accompanied by winding of the axion angle from 0 to π , leading to the half-quantized Witten effect observed before. This is nothing but the Z_2 topological glass. For the cut C, on the other hand, the situation is more interesting and involved. While, not surprisingly, again the trivial atomic insulator is stable to very small $r_o > 0$, the spectral gap closes as r_o is increased. However, the IPR calculations show that the states are not extended (see Appendix. D). This therefore is a gapless localized phase similar to an Anderson insulator. On increasing r_o further, the mobility edges which had developed inside the two “bands” meet at the Fermi level, leading to a metallic state with delocalized bulk states at the Fermi level as confirmed by our IPR results. This metallic phase thus has finite conductance. It is interesting to note that the orbital-resolved spectral weights change their character inside the metal (Fig. 4) such that when the spectral gap opens up on further increase of r_o we get the inverted gap and we are back

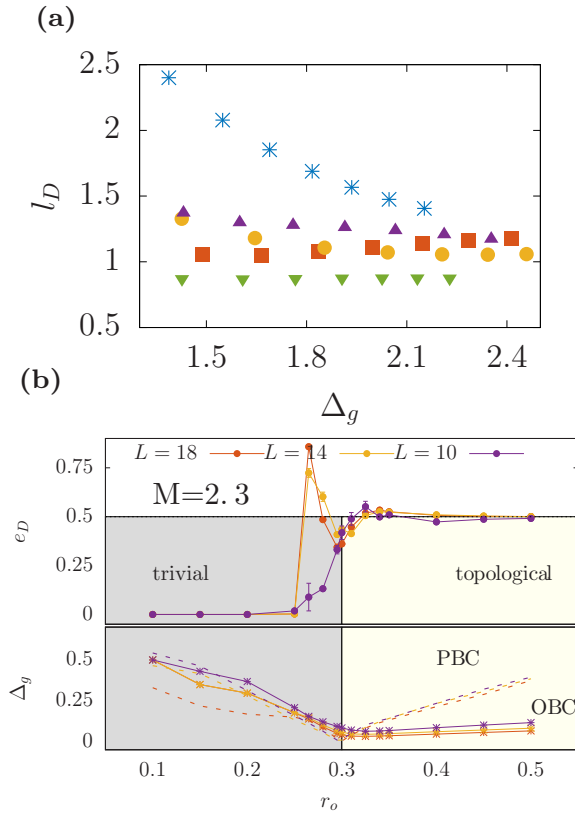


FIG. 5. Dyon length: (a) Variation of dyon length (l_D) for a sphere of amorphous TI and the corresponding spectral gap Δ_g when it is embedded as the periodic cubic amorphous TI for different choice of configurations (denoted by different point types) for various choices of $\{M, r_o\}$, broadly showing that dyon length falls with increasing band gap ($L = 16$). Note that $l_D \ll L$. (b) Variation of the dyon charge e_D as a function of r_o showing a transition from a trivial spectral insulator to a topological glass phase for another configuration of atoms at $M = 2.3$ [also see Fig. 2(d)].

in the Z_2 topological glass. It is pertinent to note that while undergoing a transition from a trivial to a topological phase does open a metallic phase in this later parameter regime (cut C), similar to the effect of disorder observed in the clean lattice systems that, however, is not always necessary (e.g., in cut B of Fig. 4).

V. ASSOCIATED PHASE TRANSITIONS

We now briefly discuss the nature of phase transitions in this system for cuts B and C, where r_o is smoothly increased. Note that this does not change the connectivity or the coordination number of the sites in a particular configuration. However, increasing r_o leads to the increase in the strength of hopping compared to the mass scale M and this destabilizes the trivial spectral insulator when the hopping energy scale becomes comparable to the mass scale [see the schematic Fig. 4(a)]. A naive estimate of the scaling relation is obtained by comparing the hopping amplitude integrated over a sphere of radius R with the mass scale $|3 - M|$. This therefore opens up a fan around $M = 3$ such that below the scale $r_o \sim |3 - M|^{1/3}$ (for $R \gg r_o$, see dashed line in Fig. 1) such that below

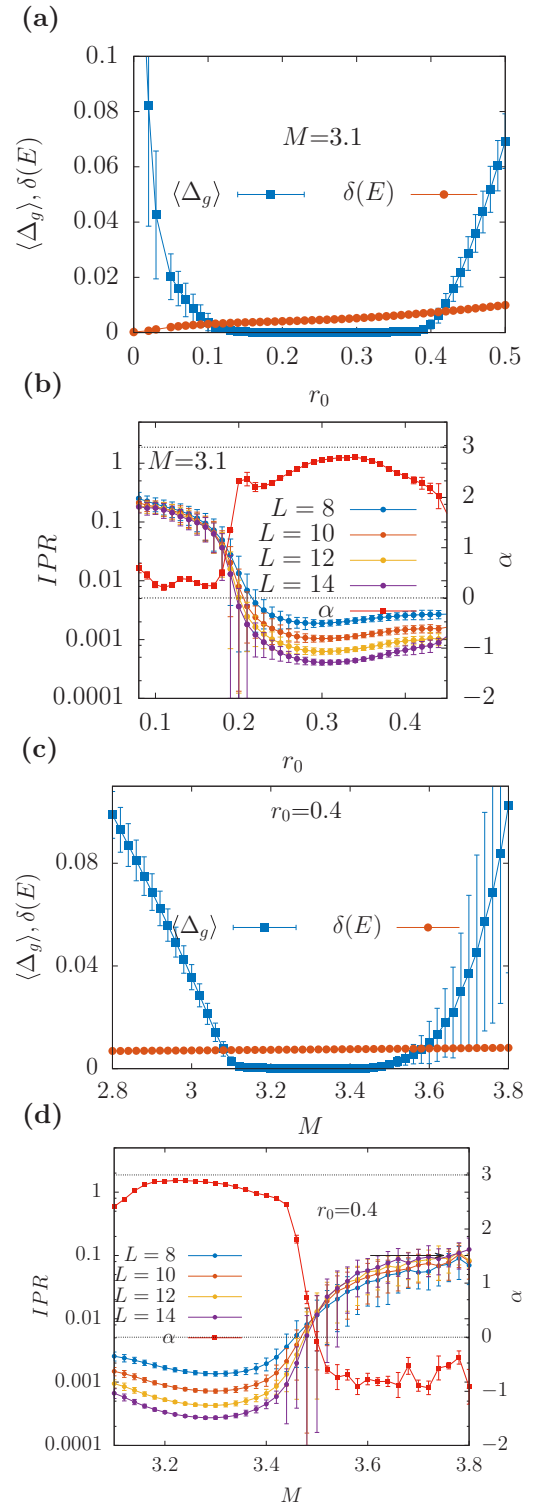


FIG. 6. Metal-insulator transitions: Configuration-averaged spectral gap Δ_g and $\delta(E)$ (see text) as a function of (a) r_o at $M = 3.1$ and (c) M for $r_o = 0.4$. IPR and their scaling exponent with system size (α) for the states near the Fermi energy are correspondingly given in (b) and (d) ($N_c = 200$).

this scale, trivial spectral insulator survives as a stable phase and gives way to other phases above it.

Moving out of the Z_2 insulator, our numerical calculations reveal that the bulk gap closing leads to either a metal or a

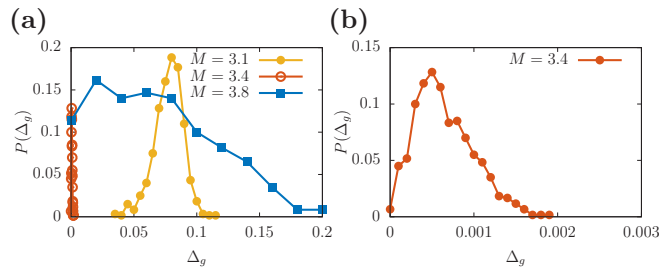


FIG. 7. Distribution of spectral gap: Regions in the parameter space have different distribution of spectral gaps. (a) For $r_o = 0.5$, $M = 3.1, 3.4, 3.8$ are shown. In the metallic phase, i.e., at $M = 3.4$, the distribution is narrow which is zoomed in (b) ($R = 2$, $L = 10$, $N_c = 600$).

trivial spectral insulator. For $M < 3$ we find a direct transition between the trivial and topological phases *without* an intermediate metallic phase (up to our numerical accuracy). As shown in Fig. 4, this occurs due to immediate opening up of the spectral gap along with the concomitant inversion of the orbital nature of the highest occupied state. We note that in the present way of parametrizing the system, the orbital character of the occupied bands changes as a function of M at $M = 3$ for $r_o = 0$. Thus, in cut B when one tunes r_o to reach the topological phase, the orbital character of all the occupied states (particularly much below the Fermi level) need not change. On the other hand, as the system makes a transition from a point near $M > 3$, $r_o = 0$ to the topological phase, the orbital character of the occupied bands changes in a significant way. The total variation in the orbital character of the occupied states is shown in Fig. 9. This closure of the gap and the associated untwisting of the wave function is then similar to the plateau transition in the integer quantum Hall effect [67,68]. In the majority of the region $M > 3$, however, the trivial insulator mostly gives way to a gapless phase which is either a metal with delocalized electronic states near the Fermi level or a novel Anderson insulator with properties dominated by rare region physics. We find that this transition is rather generically expected for an amorphous network. To check this, we investigate the physics of a different “control” Hamiltonian where $T_{\alpha\beta}$ is changed to a trivial form such that it does not wind around in real space (as discussed in Appendix E) keeping the onsite term unchanged and keeping the time-reversal symmetry intact. This model in a crystalline limit hosts no topological phases, and in an amorphous setting

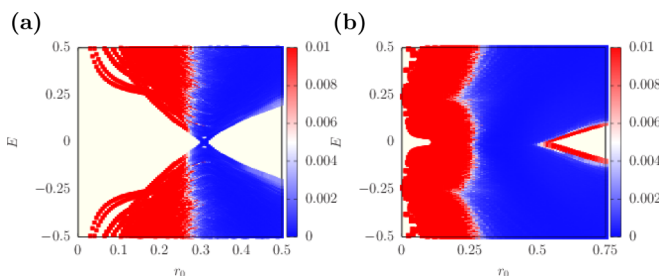


FIG. 8. Variation of IPR: Shown in (a) and (b) is the behavior of the energy spectrum as a function of r_o for a particular periodic configuration at $M = 2.2$ and 3.24 . The color bar shows the IPR of each of the states ($R = 2$, $L = 14$).

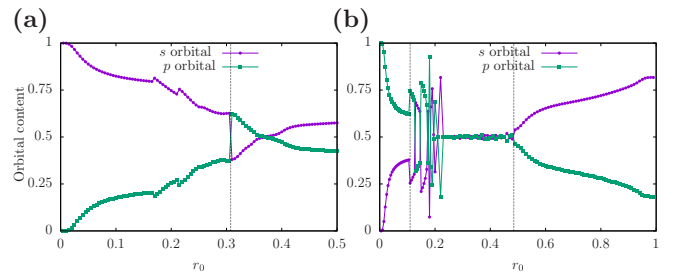


FIG. 9. Variation of orbital character: Shown in (a) and (b) is the behavior of the orbital content of the filled states as a function of r_o for a particular periodic configuration at $M = 2.2$ and 3.24 ($R = 2$, $L = 14$).

has a transition at $M = 3$, $r_o = 0$ between two atomic limits. This transition fans out to a metallic phase at finite r_o near $M = 3$ (see Appendix E). However, in contrast to this control Hamiltonian our gapless metallic phase hosts a characteristic shift in the orbital character of the states near the Fermi energy, in order to open up into a topologically nontrivial phase [see Fig. 4(b)].

VI. SUMMARY AND OUTLOOK

We have investigated the nature of phases and phase transitions for a model of a hopping Hamiltonian (introduced in Ref. [9]) which can host a topologically glassy phase. We have used the effective hopping range r_o and the onsite orbital energies (M) as effective parameters to explore the phase space. We find a rich phase diagram with a wide regime of the system being in the topological phase with interesting intermediate phases and phase transitions. We characterize the system using exact diagonalization techniques and by investigating the properties of the wave functions. In particular, we characterize the topological (and trivial) phase through the occurrence (or absence) of Witten effect. We build a comprehensive understanding of the phase diagram by alluding to ideas in the disorder literature and by examining the orbital character of the occupied orbitals in this system. We further point out that few transitions in this system could be of a distinct character than those Anderson transitions which could otherwise be found in amorphous networks. It would be an interesting future direction to completely characterize such transitions and their dependence on the symmetries, depending if they belong to a particular Altland-Zirnbauer class of the 10-fold way [2,3,69,70].

ACKNOWLEDGMENTS

We acknowledge fruitful discussions with V. B. Shenoy and S. Banerjee. A.A. acknowledges the many enlightening discussions with V. B. Shenoy and the particular collaboration [9] where many of these ideas had germinated. P.M. acknowledges funding from CSIR, India, through Shyama Prasad Mukherjee Fellowship. A.A. and S.B. acknowledge funding from Max Planck Partner Grant at ICTS. S.B. acknowledges SERB-DST (India) for funding through project Grant No. ECR/2017/000504. Numerical calculations were performed on clusters *boson* and *tetris* at ICTS. We acknowledge

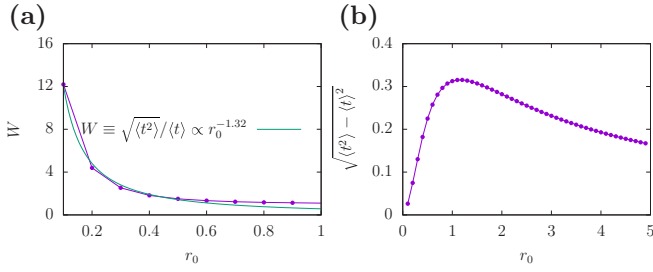


FIG. 10. Disorder estimate: Behavior of mean, standard deviation of $t(r)$ of an amorphous network ($R = 2$) and the effective disorder scale ($\equiv W$) for an amorphous network in $L = 16^3$ system as a function of r_o .

support of the Department of Atomic Energy, Government of India, under Project No. 12-R&D-TFR-5.10-1100.

APPENDIX A: HAMILTONIAN AND SYMMETRIES

Following Ref. [9] the form of the Hamiltonian is given by $\text{diag}\{-3 + M, -3 + M, 3 - M, 3 - M\}$ for on-site term and

$$T_{\alpha\beta}^{\sigma\sigma'}(\hat{r}) = \begin{pmatrix} 1 & 0 & -i \cos \theta & -ie^{-i\phi} \sin \theta \\ 0 & 1 & -ie^{i\phi} \sin \theta & i \cos \theta \\ -i \cos \theta & -ie^{-i\phi} \sin \theta & -1 & 0 \\ -ie^{i\phi} \sin \theta & i \cos \theta & 0 & -1 \end{pmatrix}, \quad (\text{A1})$$

where θ and ϕ are polar and azimuthal angle, respectively, for \mathbf{r}_{IJ} , which is the relative vector from site I to site J [see Fig. 1(a)]. More generally, the structure of $T_{\alpha\beta}^{\sigma\sigma'}$ is constrained due to symmetries. For instance, time reversal which is an antiunitary symmetry that acts on the fermionic operators as $\mathcal{T}c_{I\sigma}\mathcal{T}^{-1} = \sigma c_{I\sigma}$ constrains $T_{\alpha\beta}^{\sigma\sigma'}(\theta, \phi) = [T_{\alpha\beta}^{\bar{\sigma}\bar{\sigma}'}(\theta, \phi)]^* \bar{\sigma} \bar{\sigma}'$. Moreover, Hermiticity demands $T_{\alpha\beta}^{\sigma\sigma'}(\theta, \phi) = [T_{\alpha\beta}^{\sigma\sigma'}(\pi - \theta, \phi - \pi)]^\dagger$.

APPENDIX B: DETAILS ABOUT THE WITTEN EFFECT

In order to observe the Witten effect, the following protocol is followed. A magnetic monopole, corresponding to a vector potential $\mathbf{A} = \frac{g}{r \sin \theta} (1 + \cos \theta) \hat{\phi}$, is placed at the center of an amorphous glass sphere of diameter L (as shown in Fig. 2). g is the magnitude of the monopole strength which we fix to 1. This leads to additional Peierls phase terms on the different hoppings [see Eq. (1)]. Local electronic charge density is calculated for a half-filled system both with ($m = 1$) and without ($m = 0$) the magnetic monopole. The local difference in charge density at site I is given by $\Delta\rho(\mathbf{r}_I) = \rho(\mathbf{r}_I)_{m=1} - \rho(\mathbf{r}_I)_{m=0}$ where $\rho(\mathbf{r}_I)_{m=0(1)} = \sum_{n \in \text{occ}} \sum_{\alpha, \sigma} |\psi_n^{m=0(1)}(I, \alpha \sigma)|^2$. n labels all the eigenstates which are occupied, α is the spin/orbital index, and \mathbf{r}_I is the real-space position vector of site I where the redistributed charge density is evaluated. A finite-sized system leads to inadvertent hybridization of boundary modes, in which case it is technically prudent to keep one additional state (above

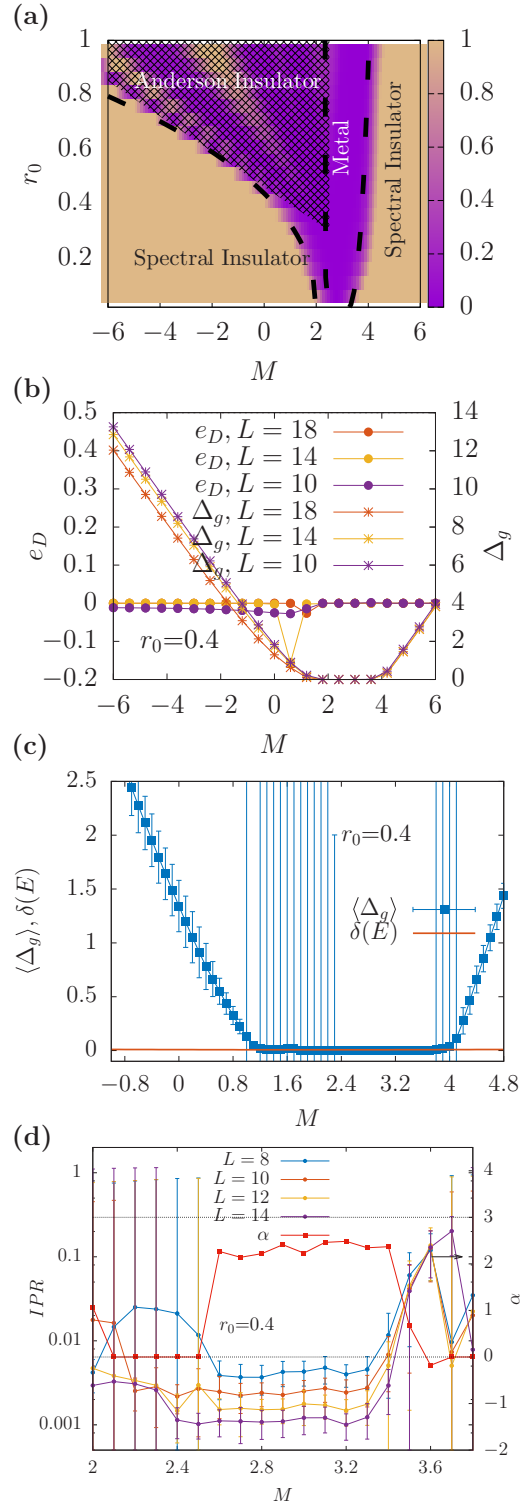


FIG. 11. Control case: (a) Configuration-averaged spectral gap in the M - r_o plane for 20 configurations ($L = 10$). Dashed lines are guide to eye. The behavior of the phase is shown in various regions. Variation of spectral gap and IPR of the states near Fermi energy is shown in (c) and (d) as a function of M for $r_o = 0.4$ ($R = 2$). The large fluctuations in Δ_g and IPR are characteristic of the Anderson localized regime. Dyon charge (e_D) and the corresponding spectral gap for a particular amorphous sphere is shown in (b) showing absence of any topological regime.

the occupied states) in calculation of density for both with and without the monopole. In order to calculate the effective change in charge density around the point where the magnetic monopole is introduced, one can evaluate the effective electric charge around the monopole using $Q_D(r) = \int_{|\mathbf{r}'|=0}^r d^3\mathbf{r}' \Delta\rho(\mathbf{r}') = \sum_{|\mathbf{r}_i| \leq r} \Delta\rho(\mathbf{r}_i)$ where r is the distance from the origin. A variation of $Q_D(r)$ as a function of r is shown in Fig. 2. We remark here that while existence of Witten effect by itself occurs rather sharply, the dyon length [see Fig. 2(b)] is configuration dependent. We observe that generally dyon length is smaller if the corresponding periodic system has a larger spectral gap (Δ_g) (see Fig. 5(a)). This is expected behavior since dyon length is expected to diverge as we go close to a quantum phase transition where the spectral gap goes to zero.

APPENDIX C: IPR, SPECTRAL GAP, AND ORBITAL CHARACTER

At any value of (M, r_o) , one can calculate the configuration-averaged spectral gap and the IPR of the states near the Fermi energy, if any. The behavior of such states was shown in Fig. 3. We provide further results for two different parameter regimes in Fig. 6. We further point out that the distribution of the spectral gap depends on which phase we are in. For instance, in near to rare-region dominated SI the distribution of spectral gaps is extremely wide (see Fig. 7). We also show the IPR of the energy spectrum and its behavior with r_o corresponding to cuts B and cut C (as discussed in Figs. 1 and 4) in Fig. 8. In Fig. 9 we show the variation of the total orbital character of the occupied states for the two cuts. While at $r_o = 0$ the system has a unique orbital polarization, with increase in r_o the two polarizations mix. In Fig. 9(a) ($M = 2.2$) there is a discontinuous jump when the gap closes, while in Fig. 9(b) ($M = 3.24$) where there is an intervening metallic regime the orbital characters are relatively equal in strengths before a band inversion occurs.

APPENDIX D: DISORDER ESTIMATE

An amorphous network, as discussed here, incorporates two “kinds” of disorder scale: one, in terms of random connectivity and therefore the fluctuation of coordination number of the sites; the second, as the distribution of hopping strengths themselves. While R decides the former, r_o determines the latter [see discussion near Eq. (1)]. Therefore, keeping R fixed one can tune r_o to change the effective disorder scale in the system $W \equiv \sqrt{\langle t^2 \rangle} / \langle t \rangle \propto r_o^{-3/2}$. For a given configuration, we numerically calculate this value whose behavior is shown in Fig. 10. A sharp upward rise in effective W is noticed in the range of $r_o \sim 0.25$ which is the scale where complete localization of all the states can be expected.

APPENDIX E: CONTROL CASE

Note that Eq. (A1) when implemented in a cubic crystalline system leads to $H = (\mathbf{1} \otimes \tau_z)[-3 + M + \cos k_x + \cos k_y + \cos k_z] + (\sigma_x \otimes \tau_x)[\sin k_x] + (\sigma_y \otimes \tau_x)[\sin k_y] + (\sigma_z \otimes \tau_x)[\sin k_z]$ which realizes a three-dimensional Dirac cone at $M = 0$. We consider a deformed $H = (\mathbf{1} \otimes \tau_z)[-3 + M + \cos k_x + \cos k_y + \cos k_z] + (\sigma_x \otimes \tau_x)[\sin k_x + \sin k_y + \sin k_z]$.

On a random lattice we generalize this to $T_{\alpha\beta}^{\sigma\sigma'}(\hat{r}) = -i\{[\cos(\phi) + \sin(\phi)]\sin(\theta) + \cos(\theta)\}(\sigma_x \otimes \tau_x)$. This respects time-reversal symmetry and Hermiticity. We analyze the phases of this model in the r_o - M plane. We find an intermediate metallic phase near $M \sim 3$ between two spectral insulator phases. This can be seen in Fig. 11 which shows the IPR, Δ_g , and Witten effect in this system for a variety of parameters. Importantly, this has no topological regime since the system shows no Witten effect. This, however, can be understood from the fact that, unlike this control case, $T_{\alpha\beta}^{\sigma\sigma'}(\hat{r})$ in the topological case equals $\mathbf{1} \otimes \tau_z - i\hat{r} \cdot \boldsymbol{\sigma} \otimes \tau_x$ [see Eq. (A1)] which winds around on a real-space sphere.

-
- [1] X.-G. Wen, *Rev. Mod. Phys.* **89**, 041004 (2017).
 [2] A. W. W. Ludwig, *Phys. Scr.* **T168**, 014001 (2016).
 [3] C.-K. Chiu, J. C. Y. Teo, A. P. Schnyder, and S. Ryu, *Rev. Mod. Phys.* **88**, 035005 (2016).
 [4] M. Z. Hasan and C. L. Kane, *Rev. Mod. Phys.* **82**, 3045 (2010).
 [5] X.-L. Qi and S.-C. Zhang, *Rev. Mod. Phys.* **83**, 1057 (2011).
 [6] Y. Ando, *J. Phys. Soc. Jpn.* **82**, 102001 (2013).
 [7] K. Yang, W. Setyawan, S. Wang, M. Buongiorno Nardelli, and S. Curtarolo, *Nat. Mater.* **11**, 614 (2012).
 [8] M. Vergniory, L. Elcoro, C. Felser, B. Bernevig, and Z. Wang, *Nature (London)* **566**, 480 (2019).
 [9] A. Agarwala and V. B. Shenoy, *Phys. Rev. Lett.* **118**, 236402 (2017).
 [10] N. P. Mitchell, L. M. Nash, D. Hexner, A. M. Turner, and W. T. M. Irvine, *Nat. Phys.* **14**, 380 (2018).
 [11] R. Shindou and S. Murakami, *Phys. Rev. B* **79**, 045321 (2009).
 [12] B. Leung and E. Prodan, *Phys. Rev. B* **85**, 205136 (2012).
 [13] K. Kobayashi, T. Ohtsuki, and K.-I. Imura, *Phys. Rev. Lett.* **110**, 236803 (2013).
 [14] J. Song, C. Fine, and E. Prodan, *Phys. Rev. B* **90**, 184201 (2014).
 [15] S. Ryu and K. Nomura, *Phys. Rev. B* **85**, 155138 (2012).
 [16] B. Sbierski and P. W. Brouwer, *Phys. Rev. B* **89**, 155311 (2014).
 [17] T. Ohtsuki and T. Ohtsuki, *J. Phys. Soc. Jpn.* **86**, 044708 (2017).
 [18] Y. Akagi, H. Katsura, and T. Koma, *J. Phys. Soc. Jpn.* **86**, 123710 (2017).
 [19] E. Prodan, T. L. Hughes, and B. A. Bernevig, *Phys. Rev. Lett.* **105**, 115501 (2010).
 [20] H.-M. Guo, G. Rosenberg, G. Refael, and M. Franz, *Phys. Rev. Lett.* **105**, 216601 (2010).
 [21] E. Prodan, Disordered topological insulators: A brief introduction, in *A Computational Non-commutative Geometry Program for Disordered Topological Insulators* (Springer, Cham, 2017), pp. 1–9.
 [22] H. Huang and F. Liu, *Phys. Rev. Lett.* **121**, 126401 (2018).
 [23] Z. Li and R. S. K. Mong, *Phys. Rev. B* **100**, 205101 (2019).

- [24] C. Bourne, A. L. Carey, and A. Rennie, *Rev. Math. Phys.* **28**, 1650004 (2016).
- [25] T. A. Loring, *Ann. Phys.* **356**, 383 (2015).
- [26] E. Prodan and H. Schulz-Baldes, Monograph in Springer Series in Mathematical Physics Studies, (Springer, 2016).
- [27] A. M. Essin and J. E. Moore, *Phys. Rev. B* **76**, 165307 (2007).
- [28] E. Prodan and H. Schulz-Baldes, *J. Funct. Anal.* **271**, 1150 (2016).
- [29] J. Li, R.-L. Chu, J. K. Jain, and S.-Q. Shen, *Phys. Rev. Lett.* **102**, 136806 (2009).
- [30] T. A. Loring and M. B. Hastings, *Europhys. Lett.* **92**, 67004 (2010).
- [31] Z. Wang and S.-C. Zhang, *Phys. Rev. X* **4**, 011006 (2014).
- [32] H.-M. Guo, *Phys. Rev. B* **82**, 115122 (2010).
- [33] D. Varjas, M. Fruchart, A. R. Akhmerov, and P. Perez-Piskunow, [arXiv:1905.02215](https://arxiv.org/abs/1905.02215).
- [34] I. Mondragon-Shem and T. L. Hughes, [arXiv:1906.11847](https://arxiv.org/abs/1906.11847).
- [35] A. Yamakage, K. Nomura, K.-I. Imura, and Y. Kuramoto, *Phys. Rev. B* **87**, 205141 (2013).
- [36] A. Banerjee, O. Deb, K. Majhi, R. Ganesan, D. Sen, and P. S. Anil Kumar, *Nanoscale* **9**, 6755 (2017).
- [37] B. Roy, Y. Alavirad, and J. D. Sau, *Phys. Rev. Lett.* **118**, 227002 (2017).
- [38] P. Goswami and S. Chakravarty, *Phys. Rev. B* **95**, 075131 (2017).
- [39] C. Liu, W. Gao, B. Yang, and S. Zhang, *Phys. Rev. Lett.* **119**, 183901 (2017).
- [40] T. A. Loring, *J. Math. Phys.* **60**, 081903 (2019).
- [41] G.-W. Chern, *Europhys. Lett.* **126**, 37002 (2019).
- [42] V. Peano and H. Schulz-Baldes, *J. Math. Phys.* **59**, 031901 (2018).
- [43] Y.-B. Yang, T. Qin, D.-L. Deng, L.-M. Duan, and Y. Xu, *Phys. Rev. Lett.* **123**, 076401 (2019).
- [44] P. A. Lee and T. V. Ramakrishnan, *Rev. Mod. Phys.* **57**, 287 (1985).
- [45] J. T. Edwards and D. J. Thouless, *J. Phys. C: Solid State Phys.* **5**, 807 (1972).
- [46] D. Thouless, *Phys. Rep.* **13**, 93 (1974).
- [47] B. Kramer and A. MacKinnon, *Rep. Prog. Phys.* **56**, 1469 (1993).
- [48] F. Evers and A. D. Mirlin, *Rev. Mod. Phys.* **80**, 1355 (2008).
- [49] I. Sahlberg, A. Westström, K. Pöyhönen, and T. Ojanen, [arXiv:1902.01623](https://arxiv.org/abs/1902.01623).
- [50] E. Witten, *Phys. Lett. B* **86**, 283 (1979).
- [51] F. Wilczek, *Phys. Rev. Lett.* **58**, 1799 (1987).
- [52] G. Rosenberg and M. Franz, *Phys. Rev. B* **82**, 035105 (2010).
- [53] V. Heine, *J. Phys. C: Solid State Phys.* **4**, L221 (1971).
- [54] D. Weaire and M. F. Thorpe, *Phys. Rev. B* **4**, 2508 (1971).
- [55] M. F. Thorpe and D. Weaire, *Phys. Rev. B* **4**, 3518 (1971).
- [56] R. J. Elliott, J. A. Krumhansl, and P. L. Leath, *Rev. Mod. Phys.* **46**, 465 (1974).
- [57] L. Schwartz and H. Ehrenreich, *Phys. Rev. B* **6**, 4088 (1972).
- [58] J. H. Davies, P. A. Lee, and T. M. Rice, *Phys. Rev. B* **29**, 4260 (1984).
- [59] M. N. Saha, *Phys. Rev.* **75**, 1968 (1949).
- [60] M. A. Metlitski, C. L. Kane, and M. P. A. Fisher, *Phys. Rev. B* **88**, 035131 (2013).
- [61] C. Wang, A. C. Potter, and T. Senthil, *Science* **343**, 629 (2014).
- [62] M. A. Metlitski and A. Vishwanath, *Phys. Rev. B* **93**, 245151 (2016).
- [63] J. Maciejko and G. A. Fiete, *Nat. Phys.* **11**, 385 (2015).
- [64] J. Maciejko, X.-L. Qi, A. Karch, and S.-C. Zhang, *Phys. Rev. Lett.* **105**, 246809 (2010).
- [65] B. Swingle, M. Barkeshli, J. McGreevy, and T. Senthil, *Phys. Rev. B* **83**, 195139 (2011).
- [66] S. Bhattacharjee, Y. B. Kim, S.-S. Lee, and D.-H. Lee, *Phys. Rev. B* **85**, 224428 (2012).
- [67] B. Huckestein, *Rev. Mod. Phys.* **67**, 357 (1995).
- [68] R. E. Prange, *The Quantum Hall Effect* (Springer, New York, 1987), pp. 69–99.
- [69] S. Ryu, A. P. Schnyder, A. Furusaki, and A. W. W. Ludwig, *New J. Phys.* **12**, 065010 (2010).
- [70] A. Agarwala, A. Haldar, and V. B. Shenoy, *Ann. Phys.* **385**, 469 (2017).